01 Dec 1978

# Crystalline To Amorphous Transformation In Ion-implanted Silicon: A Composite Model

John R. Dennis

Edward Boyd Hale
*Missouri University of Science and Technology*, ehale@mst.edu



## Recommended Citation

J. R. Dennis and E. B. Hale, "Crystalline To Amorphous Transformation In Ion-implanted Silicon: A Composite Model," *Journal of Applied Physics*, vol. 49, no. 3, pp. 1119 - 1127, American Institute of Physics, Dec 1978.
The definitive version is available at https://doi.org/10.1063/1.325049

RESEARCH ARTICLE | AUGUST 18 2008

# Crystalline to amorphous transformation in ion-implanted silicon: a composite model

John R. Dennis; Edward B. Hale



*Journal of Applied Physics* 49, 1119–1127 (1978)
https://doi.org/10.1063/1.325049

# Crystalline to amorphous transformation in ion-implanted silicon: a composite model[a)]

John R. Dennis[b)] and Edward B. Hale

*Department of Physics and Materials Research Center, University of Missouri—Rolla, Rolla, Missouri 65401*

(Received 9 June 1977; accepted for publication 24 October 1977)

The transformation of silicon to the amorphous state by implanted ions was studied both experimentally and theoretically. Experimentally, the amount of transformed silicon and the critical ion dose necessary to amorphize the entire implanted layer were determined by ESR. How the critical dose varies with ion mass (Li, N, Ne, Ar, and Kr), ion energy (20–180 keV), and implant temperature (77–475 K) was determined. Theoretically, several phenomenological models were used to analyze these data. The overlap-damage model was used to determine the critical dose from the data, the size of the amorphous region around the ion track, and the degree of overlap damage required for amorphization. For all implants, the first ion created only predamage, while the second or third ion into the same region caused the amorphous transformation. The critical-energy-density model was in good agreement with the measured critical doses. This model assumed that a region would become amorphous if the energy density deposited into atomic processes by the ions exceeded the critical energy density of $6\times10^{23}$ eV/cm$^3$. For high-temperature implantations, out-diffusion models can explain the temperature dependence of the critical dose. Although the analysis is not completely definitive, the critical-energy-density model may also be valid at high temperature if diffusion of the damage energy is taken into account. This out-diffusion of energy from around the ion track occurs via a thermally activated process. Probably, the energy moves with the out-diffusion of the vacancies from the ion track.

PACS numbers: 61.80.Jh, 64.70.Kb, 61.16.Hn

## I. INTRODUCTION

Crystalline silicon can be transformed into amorphous silicon by ion implantation.[1,2] This radiation-induced transformation is not observed under all implantation conditions since experimental variables, such as dose,[3] ion mass,[3–10], ion energy,[10,11] and implantation temperature,[3,5,12,13] must have appropriate values. The influence of all these variables on the amorphous transformation are systematically reported in this paper. In addition, analysis of these data has been performed and combined with concepts from several models. This combination has revealed new insight into the importance of predamage, deposited energy density, vacancy concentration and motion, and other details on the amorphization process. From these results has emerged a composite model for the basic mechanisms relevant to the amorphous transformation.

In Sec. II, the experimental results are presented. In Sec. III, the low-temperature-implantation model and analysis are discussed. At higher implantation temperatures, energy and defect diffusion become important, and the model and data for this case are analyzed in Sec. IV. Section V is a summary.

## II. EXPERIMENTAL PROCEDURES AND RESULTS

The implantations were performed on our ion accelerator with voltages from 20 to 180 kV. The samples were usually $n$-type silicon with resistivities between 10 and 100 Ω cm. They were implanted a few degrees from the [111] axis to minimize channeling effects. The samples were mounted on a rotatable Dewar, and the sample temperature could be adjusted from liquid nitrogen (80 K) to above 500 K. The dose rate was typically a fraction of a $\mu$A/cm$^2$. Recent experiments have shown there is no dose-rate dependence in the amorphization process.[14]

All the data presented in this paper were taken by electron-spin-resonance (ESR) measurements on the intensity of the $g=2.006$ ESR line observed when ions are implanted into silicon.[15] This line has also been seen in amorphous-silicon films.[16–19] Detailed studies[15,18,20] have concluded that the amorphous layer produced by ion implantation has quite similar ESR, optical, and backscattering properties as amorphous-silicon films prepared by rf sputtering or evaporation. The spin density was[15,16,19] $(7-20)\times10^{19}$ spins/cm$^3$, or about one spin per 500 atoms. The signal anneals very little below 500 K with substantial structural changes occurring by 800 K.[2,17] The microscopic structure of the paramagnetic defect has not been positively determined. The structure has usually been attributed to a "dangling bond",[16–19] possibly at the internal surface of a macroscopic void or a vacancy cluster,[21] or perhaps at an atomic mismatch region.[22]

In this paper, as elsewhere,[2,3,5] it is assumed that the intensity of the ESR line is directly proportional to the amount of amorphous silicon present in the implanted layer. This was done for several reasons. One is that the amorphous signal is not observed at the low or moderate doses where the largest number of point defects are found, but only at high doses where the number of point defects is substantially reduced or nonexistent,[8,23] and also where other techniques have determined that amorphous material is present.[2,15,18] In addition, the linewidth, line shape, and $g$ factor do not vary substantially with dose, ion, ion energy, temperature,

a)Work supported by the US Army Research Office, Research Triangle Park, N. C.

b)Present address: Halliburton Co., Research Division, Duncan, Okla. 73533.

 0021-8979/78/4903-1119$01.10  

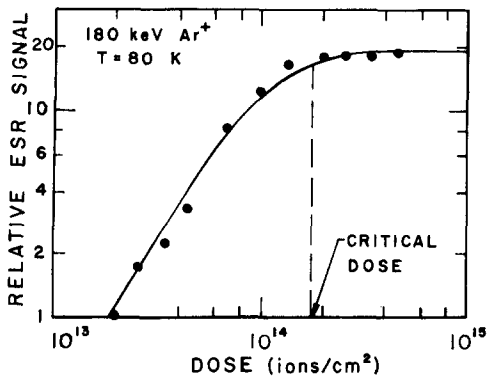


FIG. 1. Saturation of the amorphous ESR signal amplitude. The critical dose indicates the minimum dose necessary for a continuous amorphous layer.

or layer depth. These ESR parameters are rather sensitive to changes in the environment of the unpaired electron,[15,18] and their constancy suggests that the signal arises from amorphous regions which have properties very similar to the thick amorphous films or continuous implanted amorphous layer.

The ESR measurement were taken at room temperature on a $X$-band ESR spectrometer. The ESR signal was used to monitor how changes in various experimental parameters influence the amorphization process. Figure 1 shows typical data for an ESR-signal—vs-dose curve taken on a series of 11 different samples. The signal shows a strong buildup of amorphous material followed by a saturated region. The saturation indicates that the maximum number of spins have formed in the implanted layer. This is interpreted as formation of a completely amorphous layer.[2-15] In the past, a saturation dose was typically determined at the knee of the curve and was called the critical dose. As will be shown in Sec. III, the critical dose can also be determined by fitting a model (solid curve in Fig. 1) to the data points.

The critical dose can vary substantially with ion mass, ion energy, and implant temperature. For low temperature (80 K), Table I lists critical-dose values for a wide variety of implantation conditions. Table II lists values at higher temperatures. These values are all our data, some of which have been reported elsewhere.[10-12] Analysis of the dose curves, as well as systematic changes in the critical dose, yield a variety of details about the amorphization process. These details are discussed in the remainder of this paper.

TABLE I. Critical amorphizing dose at low temperature (80 K). These doses were determined from ESR data as discussed in the text. The critical doses are given in units of $10^{14}$ ions/cm$^2$ with an estimated error of ± 30%.

| Energy (keV) \ Ion | Li | N | Ne | Ar | Kr |
|---|---|---|---|---|---|
| 20 | 16 | 3.2 | 3.8 | 1.4 | 0.50 |
| 30 | | | | | 0.45 |
| 40 | 20 | 3.2 | | | 0.42 |
| 50 | | | | 1.6 | 0.40 |
| 60 | 28 | | | | |
| 80 | 42 | | | | |
| 100 | 45 | | 3.0 | 2.0 | 0.28 |
| 120 | | 5.5 | | | |
| 150 | | 4.7 | | | |
| 180 | 60 | 6.0 | 4.0 | 1.8 | 0.30 |

TABLE II. Critical amorphizing dose at higher temperatures (>200 K). These doses were determined from ESR data as discussed in the text. The critical-dose estimated error limits are ± 30%.

| Ion | Energy | $T$ (K) | Critical dose ($10^{14}$ ions/cm$^2$) |
|---|---|---|---|
| Li | 20 | 300 | >10 |
| B | 180 | 300 | 12 |
| N | 20 | 200 | 6.0 |
| | 20 | 300 | 30 |
| | 20 | 355 | 60 |
| | 20 | 381 | 85 |
| | 20 | 390 | 105 |
| | 20 | 410 | 115 |
| | 40 | 300 | 30 |
| | 60 | 300 | 42 |
| | 80 | 300 | 47 |
| | 100 | 300 | 55 |
| | 120 | 300 | 68 |
| | 180 | 300 | 85 |
| Ne | 20 | 300 | 10 |
| | 40 | 300 | 12.5 |
| | 80 | 300 | 17.5 |
| | 120 | 300 | 22.5 |
| | 180 | 300 | 25.0 |
| Ar | 20 | 200 | 1.6 |
| | 20 | 300 | 4.0 |
| | 20 | 428 | 12.5 |
| | 20 | 475 | 35.0 |
| | 20 | 508 | 70 |
| | 20 | 684 | 270 |
| Kr | 20 | 300 | 0.55 |

## III. MODELS AND ANALYSIS FOR LOW-TEMPERATURE IMPLANTATIONS

### A. Overlap-damage model

#### 1. Model

As an ion comes to rest in the sample, it produces silicon knock-ons which cause substantial radiation damage around the ion track. This damage can result in amorphization. The temperature dependence of the critical dose indicates that amorphous silicon nucleates around the ion track.[14] However, there is uncertainty as to whether a light ion, or any ion, can produce amorphous material directly, or whether the nucleating ion must strike a region which has been previously damaged. This uncertainty can be resolved by considering how the amorphous material is builtup as the implantation proceeds.

Gibbons[2] has considered the buildup of amorphous material due to overlapping damage. He showed that the amorphous fraction of the total implanted area $A_A/A_0$ can be derived from a set of differential equations which relate the differential buildup of amorphous material with dose $dA_A/d\Phi$ to the amorphous cross-sec-

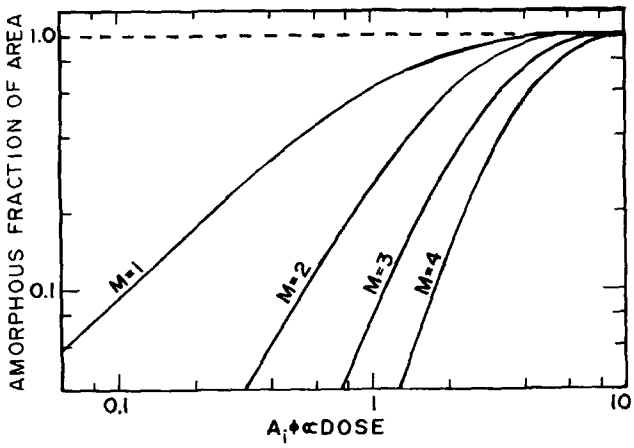


FIG. 2. Predictions of amorphous-silicon buildup with dose. The model is from Gibbons (Ref. 2). The $m$ values correspond to the number of ions necessary to damage a given region before it becomes amorphous.

tional area $A_i$ formed around the track by an amorphizing ion. The fractional amorphous area is[2]

$$\frac{A_A}{A_0} = 1 - \left( \sum_{k=0}^{m-1} \frac{(A_i\Phi)^k}{k!} \exp(-A_i\Phi) \right). \quad (1)$$

The summation-limiting integer $(m-1)$ is called the overlap number, while $m$ itself is the number of ions required to damage the same region to produce amorphization. For example, the case $m=1$ corresponds to direct amorphization by the first ion into an undamaged region. A plot of Eq. (1) for several $m$ values is shown in Fig. 2.

The above model is overly simplified. For example, $A_A$ is a function of depth into the sample if the damage profile is not uniform. (Depth-profiling results and models will be discussed elsewhere.[24]) In addition, $A_i$ and $m$ are clearly statistical averages. There are also other limitations in the differential equations used in the formulation and these are discussed in the Appendix.

### 2. Approach to complete amorphization

The importance of overlap damage can be assessed from the shape, basically the slope, of the damage curve as Fig. 2 shows. A slope greater than unity indicates that overlap damage is important in the transformation. The degree of overlap in the actual data can be determined by overlaying data curves, such as in Fig. 1, onto Fig. 2. The amorphizing ion integer $m$ can be determined using this graphical-overlay method by matching the data curve to the best-fitting curve in Fig. 2. For example, the solid curve in Fig. 1 is the $m=2$ curve. Table III lists the best-fit $m$ values to our other data. [This graphical method provides a good systematic means of analyzing the data. However, the model, Eq. (1), has its limitations as discussed in detail in the Appendix.]

The values in Table III show no definite trend in $m$ values with ion mass or ion energy, although there may be a slight decrease with mass. In some cases, whether $m=2$ or $m=3$ corresponds to the best fit is not clear because of scatter in the data. However, in all cases, the $m=1$ curve is a very bad fit to the data. (Note the substantial difference in Fig. 2 between the $m=1$ curve and the other curves, whereas the higher $m$ curves are much closer together.) Others have also observed,[5,23] the greater than linear slope, i.e., $m>1$. The above analysis, as well as a somewhat more general analysis discussed in the Appendix, strongly suggest that predamage is necessary for amorphization over a wide range of implantation variables, which includes heavy as well as light ions.

### 3. Critical dose

Each critical-dose value listed in Tables I and II was determined as the dose at 90% of the saturated-signal value using a graphical overlay of Fig. 2 to fit the data. Figure 1 shows this method more or less yields typically quoted values for the "knee" of "lowest-saturation" dose.[25]

### 4. Size of amorphous region

In the graphical-fitting process, the dose axis of a curve like Fig. 1 calibrates the $x$ axis of Fig. 2. Thus, the amorphous area $A_i$ can be determined. In the past,[3] it has often been assumed that the critical dose was the reciprocal of $A_i$, since $A_i$ is the amorphized area per

TABLE III. Amorphizing ion number for various ions and energies as obtained from comparing shape of dose curve to overlap-model curves.

| Temperature | 80 K | | | | | | 300 K | | | |
|---|---|---|---|---|---|---|---|---|---|---|
| Ion | Li | N | Ne | Ar | Kr | B | N | Ne | Ar | Kr |
| Energy (keV) | Ion number ($m$) | | | | | | | | | |
| 20 | $2\frac{1}{2}$ | 2 | 3 | 2 | 2 | | $1\frac{3}{4}$ | 2 | 2 | 2 |
| 30 | | | | | 2 | | | | | |
| 40 | 3 | 3 | | | 2 | | 3 | 3 | | |
| 50 | | | | 2 | 2 | | | | | |
| 60 | 3 | | | | | | 3 | | | |
| 80 | | | | | | | 3 | 3 | | |
| 100 | 3 | | 3 | $1\frac{3}{4}$ | 2 | | 2 | | | |
| 120 | | 2 | | | | | 2 | 2 | | |
| 150 | | 2 | | | | | | | | |
| 180 | $2\frac{1}{2}$ | 2 | 3 | $2\frac{1}{2}$ | 3 | 3 | 2 | 3 | | |

TABLE IV. Diameters of amorphous regions for low-temperature (80 K) implantations. The values are the diameters in Angstroms corresponding to a circular area $A_i$ in Eq. (1), with the $m$ values given in Table III. Values may be low as discussed in the Appendix.

| Energy (keV) \ Ion | Li | N | Ne | Ar | Kr |
|---|---|---|---|---|---|
| 20 | 6.1 | 12 | 14 | 19 | 31 |
| 180 | 3.1 | 9.0 | 13 | 18 | 48 |

ion. [This is equivalent to using a critical dose at 63% of the saturation level on the $m=1$ curve, or 27% on the $m=2$ curve (see Fig. 2).] Since the data show that the $m=2$ or 3 curve is appropriate, $A_i$ would have been too small by roughly a factor of 3 to 5 (see Fig. 2).

Table IV shows how the diameter of the amorphous area $A_i$ (assumed circular) varies with ion energy. The values in Table IV may be too small if the damaged area has a much smaller amorphous core (see the Appendix). The trends in the diameters show values from a few nearest-neighbor distances for the light ions to several lattice constants for the heavier ions.

## B. Critical-energy-density model

### 1. Model

A critical dose exists and can be systematically determined from a buildup model. In addition, the critical dose can be predicted from another model, the critical-energy-density (CED) model.[9,26] This model assumes that the transformation to the amorphous state is due to an increase in lattice energy. This energy increase comes from the energy deposited by the implanted ions in their collisions with the lattice atoms. (The energy lost in the collisions with the electrons is assumed to be unimportant to the transformation.) Presumably, as the implantation proceeds, the implanted energy produces a greater and greater collection of point defects. At the critical implanted energy, it becomes energetically favorable for the point defects to coalesce into voids and the tight tetrahedral structure which composes the amorphous state. Mathematically, it is convenient to define $E_c$ as the critical energy density, i.e., the energy which must be deposited into lattice damage per unit volume to amorphize that volume. This means the critical dose under all implantation conditions can be determined as the dose required to deposit the same $E_c$. Thus, for a uniform beam of area $A_0$ in a length $dX$,

$$\frac{N_c}{A_0}\frac{d\nu}{dX}=E_c, \tag{2}$$

where $N_c$ is the critical number of ions required, $X$ is the depth along the surface normal, and $\nu$ is the deposited restructuring energy per ion. (Normally, $\nu$ is taken as the energy lost in atomic processes per ion. This neglects the fraction of the energy loss which does not go into structural damage, e.g., some energy loss goes into the creation of phonons.) Since $N_c/A_0$ is the critical dose, Eq. (2) becomes

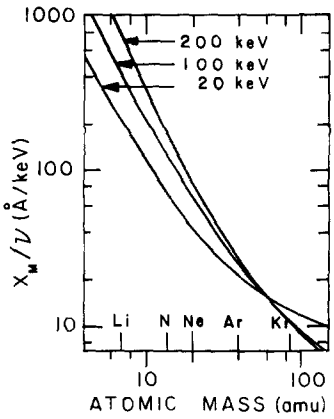


FIG. 3. Variation of $X_m/\nu$ with ion mass. The $y$-axis values were extrapolated from Ref. 28 with $X_m$ taken as the depth corresponding to 90% damage accumulation.

$$D_c=E_c\left(\frac{d\nu}{dX}\right)^{-1}. \tag{3}$$

### 2. Analysis

Since theoretical calculations are available for $d\nu/dX$, the critical dose predicted from Eq. (3) can be compared with the measured value. In principle, Eq. (3) should be verified by performing amorphous depth-profiling measurements. However, often $D_c$ is determined for the entire damaged layer and $d\nu/dX$ is approximated as $\nu/R_d$, where $R_d$ is the depth of the damage or some proportionally related depth. Thus, for a uniformly damaged layer, Eq. (3) becomes

$$D_c=E_cR_d/\nu. \tag{4}$$

Vook[26] demonstrated the importance of Eq. (4). Using data from several laboratories, he showed that the measured low-temperature critical-dose values were essentially inversely proportional to $\nu/R_d$. For $R_d$ he used the ion projected range and determined that an $E_c$ value of $6\times10^{23}$ eV/cm$^3$ fit the low-temperature data well for a variety of different ions.

Later, Dennis and Hale[11] independently verified the CED model by determining the dependence of critical dose on implantation energy. This was done for light, intermediate, and heavy ion implants. They showed that the energy dependence of the critical dose in all three cases was in good agreement with the theoretical energy dependence of $R_d/\nu$ as predicted by the model. For $R_d$ they used the quantity $X_m$, where $X_m$ was defined as the depth corresponding to 90% of the total predicted damage accumulation.

Figure 3 is a theoretical prediction of how the quantity $X_m/\nu$ varies with both mass and energy.[27,28] Values for $X_m$ and $\nu$ were extrapolated from tables.[28] These values can be compared with experiment if Eq. (4) is valid. Data points for low- and high-energy implants of $N^+$ are shown in Fig. 4. The critical dose approximately doubles between these two energies as expected from Fig. 3 and Eq. (4). Figure 5 compares the Table I data points for other ions with the solid curve predicted by Fig. 3 and Eq. (4). The vertical axis on the right was computed by assuming $E_c=6\times10^{23}$ eV/cm$^3$. Figure 5 shows the predicted and observed variation of $D_c$ with energy: an increase of $D_c$ for light ions, little change

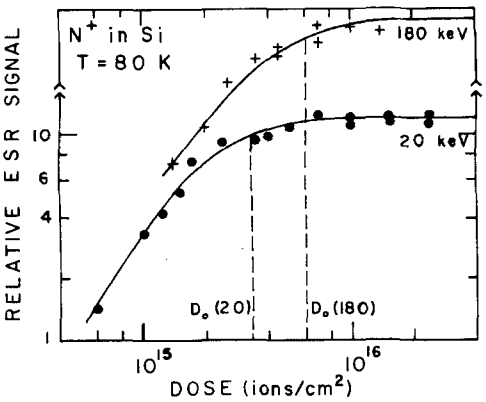


FIG. 4. Variation of the critical dose at a low and high energy for a light ion $N^+$.

with energy for intermediate ions, and decrease with energy for heavy ions.

The CED model can also be used to compute the lateral extent of the amorphization produced by the recoiling target atoms around the ion track. A recoiling secondary can be approximated as a low-energy ion implanted by the externally implanted ion. With this approximation, Eq. (4) can be used for the recoiling silicon atom. However, in this case, the projected range $R_d$ can be treated as the unknown, since an estimate for the critical dose and $\nu$ can be approximated as shown below. The importance of determining $R_d$ is that $R_d$ is related to the amorphous diameter, which was independently determined in Table IV by another calculation. The amorphous diameter is twice the component of the total range which is perpendicular to the surface. This we assume is one-half the projected range $R_d$ since the scattering is in the forward direction. This value is convenient for a first approximation since $d = R_d$. To calculate this diameter, the $\nu$ of the recoil atom is assumed to be the damage energy lost by the incoming ion between atoms,[3] i.e., $\nu_{\text{recoil}} = (d\nu/dX)_{\text{ion}} n_0^{-1/3}$, where $n_0$ is the atomic density of the target [$n_0(\text{Si}) = 5.0 \times 10^{22}$ atoms/cm$^3$]. The critical dose would correspond to about $n_0^{2/3}$, i.e., one atom per atom distance square, since the low-energy-recoil atoms primarily interact strongly with their nearest neighbors. This means the diameter can be estimated, using Eq. (4), as

$$d = \frac{n_0^{1/3}}{E_c} \left(\frac{d\nu}{dX}\right)_{\text{ion}}. \tag{5}$$

If the values in Fig. 3 are used, Eq. (5) predicts diameters of 1–3 Å for $Li^+$ and about 50 Å for $Kr^+$. These values are in very rough agreement with those independently calculated in Table IV.

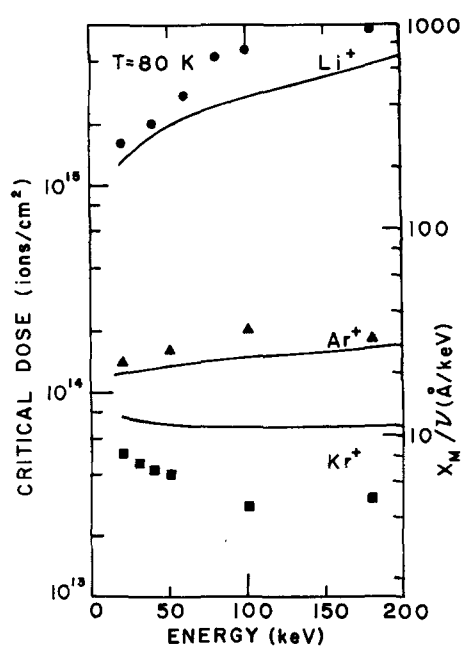


FIG. 5. Variation of the critical dose with energy for light, intermediate, and heavy ions. The solid curves correspond to $X_m/\nu$ values for Fig. 3, assuming $E_c = 6 \times 10^{23}$ eV/cm$^3$.

## IV. MODEL AND ANALYSIS FOR HIGH-TEMPERATURE IMPLANTATIONS

### A. Out-diffusion models

#### 1. Vacancy out-diffusion model

It was recognized very early that the critical dose changed substantially with implantation temperature.[29] This is especially true for light ions as Table II shows. Originally, there was some controversy over the underlying cause of this temperature dependence, but more recent work has shown that the vacancy out-diffusion model of Morehead and Crowder[3] can account for the data.[12] This model attributes the temperature dependence to thermal diffusion of vacancies radially outward from the core of the ion track for a short time interval after the ion passes.

In this short interval, various atomic rearrangements occur as the amorphous structure is being finalized. The atoms in the disordered region seek their lowest-energy configuration. Vacancy motion is likely to be important because there is a high vacancy concentration near the center of the ion track, where the vacancies were formed in the primary collisions. Some of these vacancies cluster into voids, perhaps to relieve the strain energy which builds up due to the lack of long-range order. In addition, there is also radial outward diffusion of vacancies due to the large radial gradient in the vacancy concentration. [This radial-vacancy-concentration gradient could be important because amorphous silicon is known to be several percent less dense (more voids) than crystalline silicon.] Hence, the vacancy distribution could determine the radial extent of the amorphous region. This would mean that the low-temperature (no diffusion) amorphous radius $R_0$ is decreased an amount $\delta R$ by vacancy out-diffusion. (Often $\delta R$ is not small, since for very light ions at room temperature $\delta R \approx R_0$ and no amorphous material is formed). Since the critical dose is inversely proportional to the amorphized area, the ratio of critical dose at temperature $T$ to the low-temperature critical dose can be written[3]

$$D(T)/D_0 = R_0^2/(R_0 - \delta R)^2 = [1 - (\delta R/R_0)]^{-2}. \tag{6}$$

To get the explicit temperature dependence in Eq. (6),

$\delta R$ is obtained by studying details of the vacancy out-diffusion process.

Previously,[3] the expression used for the decrease in amorphous radius $\delta R$ was

$$\delta R = 2(D_v \tau)^{1/2}$$
$$= 2[D_v^0 \tau \exp(-E/kT)]^{1/2}, \quad (7)$$

where $\tau$ is the amorphous restructuring interval and, hence, the diffusion time; $D_v$ is the vacancy-diffusion coefficient with prefactor $D_v^0$; and $E$ is the activation energy for diffusion. Such an expression for $\delta R$ was obtained from a one-dimensional diffusion equation.[3] It was not stated precisely how the solution was obtained, but for an infinitely thin plane source, the vacancy concentration drops to $e^{-1}$ of its initial value at the so-called diffusion length given by $\delta R$ in Eq. (7). Such an approximation for $\delta R$ can be improved upon as discussed below.

Another approximation is to solve for the radial concentration from a cylindrically symmetric diffusion equation assuming an initial radial Gaussian distribution for the vacancies around the ion track.[30] This distribution will decrease in amplitude and spread in width as diffusion occurs. For most implants, the critical amorphizing vacancy concentration will not be very near the peak Gaussian concentration, and this means that the amorphous radii would increase (spread) with the Gaussian distribution, and hence, the critical dose would *decrease* at the higher implantation temperatures. This has not been observed in any experiments. Since the critical dose increases (radius decreases), it is proposed that there is a sink for the vacancies at radii exceeding $R_0$. In reality, the sink would correspond to trapping by the peripheral interstitials which were knocked out to form the vacancies.

As a practical compromise, we have solved the radial-diffusion equation with an initially constant concentration out to the radius $R_0$, assumed an infinite sink for all time for greater radii (i.e., $C_v = 0$ for $R \geq R_0$), and assumed a critical concentration of $e^{-1}$ times the initial peak value. The results of the calculations are shown by individual points in Fig. 6, where the fractional loss in radius is plotted versus the normalized $D_v\tau$ product. The square-root dependence of Eq. (7) is given by the solid line. Since the experimental data vary significantly only for large $\delta R/R_0$, a better fit to the solution is a linear $D_v\tau$ approximation. With this approximation, Eq. (6) becomes

$$D(T)/D_0 = [1 - C \exp(-E/kT)]^{-2}, \quad (8)$$

where $C$ is independent of temperature. The previous equation for $D(T)/D_0$ obtained using Eq. (7) was

$$D(T)/D_0 = [1 - C' \exp(-U/kT)]^{-2}, \quad (9)$$

where $C'$ is independent of temperature and $U = \frac{1}{2}E$ because the square-root dependence in $\delta R$ introduced a factor of $\frac{1}{2}$ in the exponential. A comparison of Eqs. (8) and (9) will be made in Sec. IV B.

### 2. Energy out-diffusion model

Equation (8) can be derived from a different perspective. From this point of view, the amorphous transformation is determined by the amount of deposited atomic-energy density at all temperatures rather than just low temperatures. At high temperatures, the out-diffusion of energy from the damaged area must be considered since this diffusion reduces the energy density in the damaged region. Thus, only the central part of the damaged region transforms.

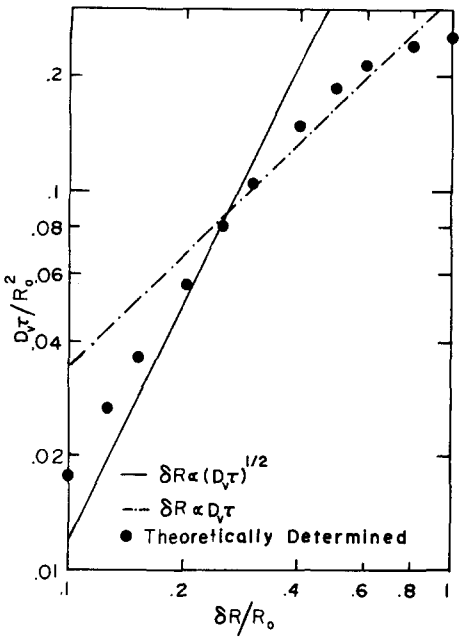


FIG. 6. Decrease in the normalized radius with increase in diffusion. The points correspond to solutions of the cylindrical diffusion equation as described in the text. The best fit at small radii (large $\delta R/R_0$) is linear in $D_v\tau$.

It is convenient to envision a plot of the deposited atomic-energy-density contours about the ion track. At low temperature, the area inside the critical-energy-density contour $E_c$ will be amorphous. For high-temperature implants, the critical-energy-density contour will contract about the ion track as the energy out-diffuses. Thus, only a smaller area will be amorphous.

A possible way for the energy to out-diffuse is via vacancies which take their energy of formation with them. If this is true, then the derivation of Eq. (8) from Eq. (6) and the cylindrical geometry equivalent of Eq. (7) is still valid. If the energy out-diffusion is proportional to vacancy out-diffusion, then Eqs. (8) and (6) are still valid. Further discussion of the models is included in Sec. IV B.

## B. Analysis of high-temperature data

### 1. Temperature dependence

Equations (8) and (9) have an identical and experimentally verified temperature dependence.[3,5,12] Figure 7 shows the data points for the case of 20-keV $Ar^+$ implants. The solid curve is Eq. (8) or (9) using a fitting procedure described elsewhere.[12] The important point is that an activated out-diffusion process can fit the data very well.

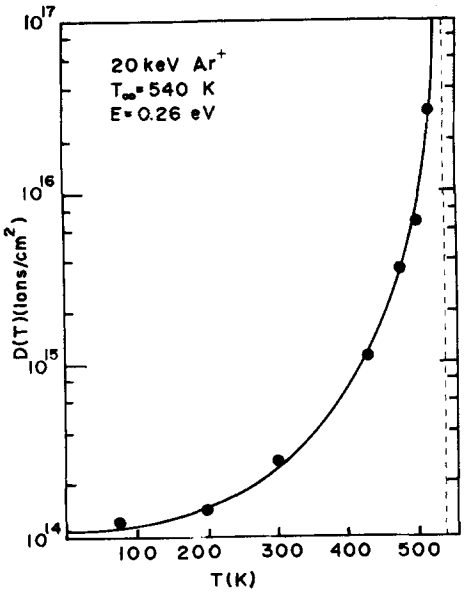


FIG. 7. Large variation of the critical dose with implantation temperature.

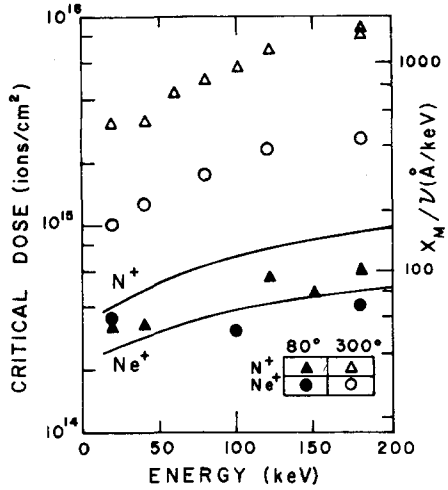


FIG. 8. Temperature variation of critical dose at various energies.

### 2. Ion-mass dependence

Although the temperature dependence cannot distinguish between Eqs. (8) and (9), the ion-mass dependence can. Namely, Eqs. (6) and (7) show that $C' \propto R_0^{-1}$, while Fig. 6 indicates $C \propto R_0^{-2}$. Since $R_0$ depends on ion mass as in Table IV, it is of interest to compare $C'^{-1}$ and $C^{-1/2}$ to $R_0$ for various ions. This is done in Table V. The comparison indicates a better agreement with Eq. (8). Hence, the experimental results support the new calculations.

Table V also lists the best-fit value for $E$ in Eq. (8). These values should ideally be the same. They seem to indicate no trend with ion mass. In addition, they are not too far from the double-negative-charge state of the vacancy, whose activation energy for migration in undamaged silicon is $0.18 \pm 0.02$ eV.[31] Other energy values exist for other charge states.[31]

Table V also lists values for $T_\infty$ defined by the equation $C = \exp(E/kT_\infty)$. (The $T_\infty$ values are easy to obtain from the data as Fig. 7 shows.)

### 3. Ion-energy dependence

Figure 8 shows high- and low-temperature data for various energies of N and Ne ions. The data suggest the energy dependence is independent of temperature despite large changes in the critical dose. This means in Eq. (6) that all the energy dependence of $D(T)$ is in $D_0$ and none in $\delta R/R_0$.

This lack of energy dependence in $\delta R/R_0$ is not understood. Some constraint seems to make the fractional area, $[1-(\delta R/R_0)]^2$, independent of energy. Since $R_0$ depends on energy (see Table IV), it is not clear why $\delta R/R_0$ does not. Perhaps the restructuring time $\tau$ makes $\delta R$ energy dependent. The vacancy out-diffusion model yields $\delta R/R_0 \propto R_0^{-2}$ [Eq. (8)] or $\delta R/R_0 \propto R_0^{-1}$ [Eq. (9)], and hence, would predict a strong energy dependence for $[1-(\delta R/R_0)]^2$. The energy out-diffusion model does not explicitly predict $\delta R/R_0$. Thus, the energy-dependence data does not conflict with this model.

## V. SUMMARY

A layer of crystalline silicon can become amorphous under certain implantation conditions. The ESR signal from the amorphous-silicon layer has been used to systematically study how the ion dose, ion mass, ion energy, and implantation temperature effect the amorphous layer formation. Analysis of the data using an overlap-damage model[2] suggested that the greater than linear buildup of amorphous material with dose occurred because the first ion into a crystalline region produced severe damage, but subsequent ions actually caused the amorphous transformation. A model called the critical-energy-density model[9,26] was used to predict the critical dose at which a complete amorphous layer is formed. This model assumed that if the energy density deposited into atomic processes exceeded the critical value ($\sim 6 \times 10^{23}$ eV/cm$^3$), then the implanted region will transform to the amorphous state. This model was able to predict the ion mass and energy dependence of the critical dose. To account for changes in the critical dose at high implantation temperature, the vacancy out-diffusion model

TABLE V. Parameters determined from the temperature dependence of the critical dose.

| Ion (20 keV) | $C^{-1/2}$ Eq. (8) ($\times 10^2$) | $C'^{-1}$ Eq. (9) ($\times 10^3$) | $R_0$ Table IV (Å) | $E$ (eV) | $T_\infty$ (K) |
|---|---|---|---|---|---|
| $N^+$ | 5.5 | 3.0 | 6 | $0.20 \pm 0.06$ | $400 \pm 30$ |
| $Ar^+$ | 6.1 | 3.7 | $9\frac{1}{2}$ | $0.26 \pm 0.06$ | $540 \pm 30$ |
| $Kr^+$ | 14.6 | 22 | $15\frac{1}{2}$ | $0.24 \pm 0.06$ | $725 \pm 30$ |

TABLE VI. Special case solution for the generalized model. Results for each case were obtained by plotting Eq. (A4) and determining the best fit $m$ and the $A_i$ values from graphical overlay comparison with results of the overlap-damage model in Fig. 2. Case 1: Gibbon's $m=1$ case; direct transformation so no intermediate damage, thus $A_d=0$. Case 2: no direct transformation so $A_a=0$. Case 2(a): Gibbons's $m=2$ case since damage and transformed areas are the same. Case 2(b) and 2(c): small transformed core approximations. Case 3: equal transformed areas so $A_a=A_c$. Case 4: very small transformed core approximation.

| Case No. | Area conditions | Best-fit $m$ value | Best-fit $A_i$ value |
|---|---|---|---|
| 1 | $A_d=0$ | 1 (exact) | $A_a$ |
| 2 | $A_a=0$ and | | |
| 2(a) | $A_d=A_c$ or | 2 (exact) | $A_c$ |
| 2(b) | $A_d=5A_c$ or | $1\frac{1}{2}$ or 2 | $A_c$ or $\frac{1}{2}A_c$ |
| 2(c) | $A_d=10A_c$ | $1\frac{1}{3}$ or 2" | $A_c$ or $\frac{1}{3}A_c$ |
| 3 | $A_a=A_c$ | 1 (exact) | $A_a=A_c$ |
| 4 | $A_d \gg (A_a-A_c)$ or $\gg$ both $A_a$, $A_c$ | 1 | $A_c$ |

has been used. At the higher temperatures, the large number of vacancies along the ion track radially diffused outward from the track. Since this out-diffusion increased the density of silicon and lowered the energy density around the track, the amount of amorphous material formed at the same dose was less for high-temperature implants than low-temperature ones. In conclusion, despite the complexity of the amorphization process, a phenomenological composite model can be used to interpret and predict critical features of importance on a microscopic level.

## APPENDIX

In Sec. III A it was shown that most of the data can be fit to Gibbon's overlap model[2] with $m=2$, i.e., the second ion into the same region causes the amorphization. In this Appendix, a more generalized model for the $m=2$ case is considered in detail. Namely, the model takes into account direct amorphous conversion from an undamaged region as well as conversion from a damaged region. The model is important because it provides a better understanding of the limitations of the method used in the main text to determine $m$ and $A_c$.

In this model it is assumed that the undamaged area $A_u$ of the total area $A_0$ is depleted during the implantation by two mechanisms. First, an area $A_d$ is converted per ion into a damaged but not amorphous region. Second, an area $A_a$ is directly converted per ion into an amorphous region. Thus, the change of the undamaged area with bombardment is

$$\frac{dA_u}{dN}=-A_a\frac{A_u}{A_0}-A_d\frac{A_u}{A_0}, \tag{A1}$$

where $A_u/A_0$ is the probability of hitting an undamaged region. The change in total damage area $A_D$ is given by

$$\frac{dA_D}{dN}=A_d\frac{A_u}{A_0}-A_c\frac{A_D}{A_0}, \tag{A2}$$

in which the first term on the right-hand side is the area builtup from the previously undamaged area, and the second term is the depletion of damaged area due to an area $A_c$, which is converted per ion to an amorphous area. Finally, the increase in total amorphous area $A_A$ from both undamaged and damaged area is

$$\frac{dA_A}{dN}=A_a\frac{A_u}{A_0}+A_c\frac{A_D}{A_0}. \tag{A3}$$

The solution for $A_A$ from Eqs. (A1)—(A3)

$$A_A=A_0\left\{1-\frac{A_d}{(A_a+A_d-A_c)}\exp-\left(\frac{A_c}{A_0}N\right)\times\left[\exp\left(-\frac{(A_a+A_d)}{A_0}\right)N\right](A_a+A_d)^{-1}\times\left(A_a-\frac{A_cA_d}{(A_a+A_d-A_c)}\right)\right\}. \tag{A4}$$

Equation (A4) is important because it predicts the shape of the dose curve once a choice for $A_a$, $A_d$, and $A_c$ has been made. A variety of choices have been considered for these areas. The results are summarized in Table VI. One result is that the experimentally determined $m$ value would normally be less than its nominal $m=2$ value. The fact that the typically observed value is 2 suggests that Gibbon's model [case 2(a)] is rather good or that the true $m$ has a higher value. In either case, the main conclusion in the text, i.e., predamage is necessary, remains valid.

The second point is that in cases such as 2(b) or 2(c), $A_i$ can be too small by a factor of perhaps 2 or 3. Such cases are not unrealistic since transmission-electron-microscope studies show individual damage regions (presumably the diameter of $A_d$) to be larger than the $A_i$ diameter values in Table IV, espeically for light ions.




[1] D. J. Mazey, R. S. Nelson, and R. S. Barnes, Philos. Mag. 17, 1145 (1968).
[2] J. F. Gibbons, Proc. IEEE 60, 1062 (1972); this article gives a review of some of the early work.
[3] F. F. Morehead and B. L. Crowder, Radiat. Eff. 6, 27 (1970).
[4] V. M. Gusev, Yu. V. Martynenko, and K. V. Starinin, Sov. Phys.-Crystallogr. 14, 908 (1970).
[5] F. F. Morehead, B. L. Crowder, and R. S. Title, J. Appl. Phys. 43, 1112 (1972).
[6] N. N. Gerasimenko, A. V. Durechensky, S. I. Romanov, and S. Smirnov, *Radiation Damage and Defects in Semiconductors*, edited by J. E. Whitehouse (Institue of Physics, London, 1972), pp. 72—80.
[7] S. Furakawa and H. Ishiwara, Jpn. J. Appl. Phys. 11, 1062 (1972).
[8] E. C. Baranova, V. M. Gusev, Yu. V. Martynenko, C. V. Starinin, and I. B. Haibullin, Radiat. Eff. 18, 21 (1973).
[9] H. Muller, K. Schmid, H. Ryssel, and I. Ruge, *Ion Implantation in Semiconductors and Other Materials*, edited by B. L. Crowder (Plenum, New York, 1973), pp. 203—214.
[10] J. R. Dennis and E. B. Hale, Radiat. Eff. 19, 67 (1973).
[11] J. R. Dennis and E. B. Hale, Appl. Phys. Lett. 29, 523 (1976).
[12] J. R. Dennis, G. K. Woodward, and E. B. Hale, *International Conference on Lattice Defects in Semiconductors* (Institute of Physics, London, 1975), pp. 467—473.
[13] E. C. Baranova, V. M. Gusev, Yu. V. Martynenko, and I. B. Haibullin, Radiat. Eff. 25, 157 (1975).
[14] J. R. Dennis and E. B. Hale, Radiat. Eff. 30, 219 (1976).

[15]B. L. Crowder, R. S. Title, M. H. Brodsky, and G. D. Pettit, Appl. Phys. Lett. **16**, 205 (1970).
[16]M. H. Brodsky and R. S. Title, Phys. Rev. Lett. **23**, 581 (1969).
[17]M. H. Brodsky, R. S. Title, K. Weiser, and G. D. Petit, Phys. Rev. B **1**, 2632 (1970).
[18]R. S. Title, M. H. Brodsky, and B. L. Crowder, *Proceeding of the Tenth International Conference on the Physics of Semiconductors*, edited by S. P. Keller, J. C. Hensel, and F. Stern (U. S. Atomic Energy Commission, Oak Ridge, Tenn. 1970), p. 794.
[19]P. A. Thomas, D. Lepine, and D. Kaplan, *Proceedings of the International Conference on Tetrahedrally Bonded Amorphous Semiconductors*, edited by M. H. Brodsky, S. Kirkpatrick, and D. Weaire (American Institute of Physics, New York, 1974), p. 47.
[20]B. L. Crowder and R. S. Title, Radiat. Eff. **6**, 63 (1970).
[21]D. Kaplan, D. Lepine, Y. Petroff, and P. Thirry, Phys. Rev. Lett. **35**, 1376 (1975).
[22]B. P. Lemke and D. Haneman, Phys. Rev. Lett. **35**, 1379 (1975).
[23]K. L. Brower and W. Beezhold, J. Appl. Phys. **43**, 3499 (1972).
[24]J. P. Sadowski and E. B. Hale (unpublished).
[25]J. C. Bourgoin, J. F. Morhange, and R. Beserman, Radiat. Eff. **22**, 205 (1974); this paper noted that the saturation dose does vary somewhat depending possibly on the measuring laboratory's experimental procedure. However, the comparison they emphasize between a Raman-scattering (RS) and ESR-saturation dose is not a valid comparison. The RS measures loss of crystallinity, while the ESR measures amorphous silicon. There is an intermediate state corresponding to amorphous predamage, i.e., noncrystalline heavily damaged silicon.
[26]F. L. Vook, *Radiation Damage and Defects in Semiconductors*, edited by J. E. Whitehouse (Institute of Physics, London, 1972), pp. 60—71.
[27]D. K. Brice, *Ion Implantation Range and Energy Deposition Distributions* (Plenum, New York, 1975), Vol. 1.
[28]K. B. Winterbon, *Ion Implantation Range and Energy Deposition Distributions* (Plenum, New York, 1975), Vol. 2.
[29]R. S. Nelson and D. J. Mazey, Can. J. Phys. **46**, 689 (1968).
[30]J. R. Dennis, Ph. D. thesis (University of Missouri-Rolla, 1976) (unpublished).
[31]G. D. Watkins, *Radiation Effects in Semiconductors*, edited by F. L. Vook (Plenum, New York, 1968), pp. 67—81.